Article

Mesophase Tuning in Discotic-Dimers #-Conjugated Ionic Liquid Crystals through Supramolecular Interactions and the Thermal History

Lucia Veltri, Vito Maltese, Finizia Auriemma, Chiara Santillo, Sante Cospito, Massimo La Deda, Giuseppe Chidichimo, Bartolo Gabriele, Claudio De Rosa, and Amerigo Beneduci

Cryst. Growth Des., **Just Accepted Manuscript** • DOI: 10.1021/acs.cgd.6b00441 • Publication Date (Web): 29 Aug 2016

Mesophase Tuning in Discotic-Dimers π-Conjugated Ionic Liquid Crystals through Supramolecular Interactions and the Thermal History

Lucia Veltri,,† Vito Maltese,† Finizia Auriemma,‡ Chiara Santillo,‡ Sante Cospito,† Massimo La Deda,† Giuseppe Chidichimo,† Bartolo Gabriele,† Claudio De Rosa,‡ and Amerigo Beneduci*†*

†Department of Chemistry and Chemical Technologies, University of Calabria, Via P. Bucci, 87036 Arcavacata di Rende (CS), Italy. ‡Department of Chemical Sciences, University of Naples Federico II, Complesso Monte Sant' Angelo, Via Cintia, 80126 Naples, Italy.

*lucia.veltri@unical.it, *amerigo.beneduci@unical.it

π-Conjugated ionic liquid crystals are a very interesting class of salts where the coupling of ionic and electronic functions with the anisotropy typical of liquid crystals may give raise to materials with advanced bulk properties. Defect-free active thin films obtainable by simple mesophase self-assembly of these materials, may be exploited in a number of different electro-optical devices. Here we show that the rich mesomorphism of the thienoviologen salts 4,4'-(2,2'-bithiophene-5,5'-diyl)bis(1-alkylpyridinium), which includes smectic, columnar and nematic phases, significantly depends on the counterion type and on the length of the promesogenic alkyl chains, highlighting the delicate balance among ion/ion, π-π stacking and hydrophobic interactions. These salts show notable fluorescence properties in the bulk, strongly dependent on the self-assembling.

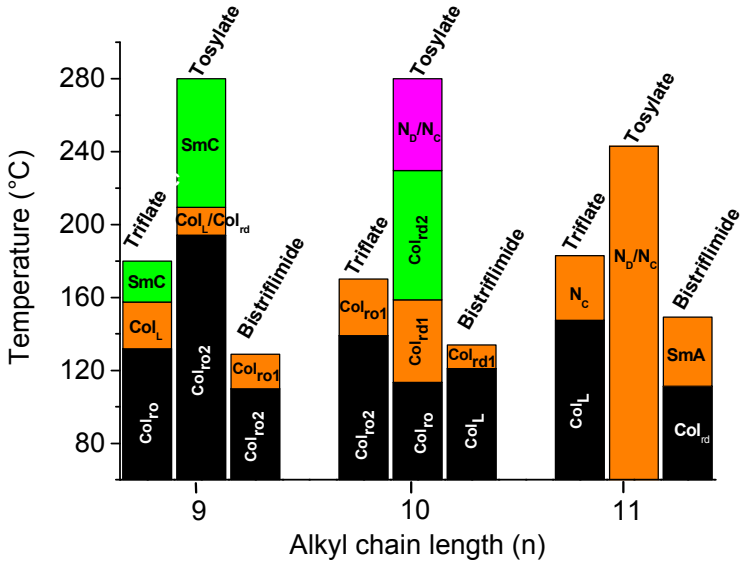

Mesophase Tuning in Discotic-Dimers π-Conjugated Ionic Liquid Crystals through Supramolecular Interactions and the Thermal History

Lucia Veltri,[†] *Vito Maltese,*[†] *Finizia Auriemma,*[‡] *Chiara Santillo,*[‡] *Sante Cospito,*[†] *Massimo La Deda,*[†] *Giuseppe Chidichimo,*[†] *Bartolo Gabriele,*[†] *Claudio De Rosa,*[‡] *and Amerigo Beneduci**[†]

†Department of Chemistry and Chemical Technologies, University of Calabria, Via P. Bucci, 87036 Arcavacata di Rende (CS), Italy. ‡Department of Chemical Sciences, University of Naples Federico II, Complesso Monte Sant' Angelo, Via Cintia, 80126 Naples, Italy.

KEYWORDS Ionic Liquid Crystals, Thienoviologen, Nematic Columnar, Nematic Discotic, Fluorescence

ABSTRACT π-Conjugated ionic liquid crystals are a very interesting class of salts where the coupling of ionic and electronic functions with the anisotropy typical of liquid crystals may give raise to materials with advanced bulk properties. Defect-free active thin films obtainable by simple mesophase self-assembly of these materials, may be exploited in a number of different electro-optical devices. Here we show that the rich mesomorphism of the thienoviologen salts 4,4'-(2,2'-bithiophene-5,5'-diyl)bis(1-alkylpyridinium), which includes smectic, columnar and nematic phases, significantly depends on the counterion type and on the length of the promesogenic alkyl chains, highlighting the delicate balance among ion/ion, π-π stacking and

hydrophobic interactions. These salts show notable fluorescence properties in the bulk, strongly dependent on the self-assembling.

INTRODUCTION

Ionic interactions[1-6] are a key noncovalent strategy to create highly ordered supramolecular assemblies with advanced materials properties.[7] Such interactions play also a fundamental role in ionic liquid crystals (ILCs) that are liquid crystalline compounds incorporating a cationic function such as imidazolium or pyridilium moieties.[8-13] In ILCs where the ionic functionality is linked to one or more promesogenic pendants (alkyl chains, benzyl substituted groups, etc.), ion-ion stacking and electrostatic interactions tend to stabilize lamellar[8] and columnar[10] mesophases due to the amphiphilic nature of these compounds. On the other hand, when a mesogenic core is linked to the ionic functionality through a spacer, besides smectic and columnar phases,[8-13] also nematic phases were recently reported in a few examples.[14-19] In such systems, excluded volume effects induced by the anisotropic core, drive the formation of the nematic phase, as opposite to the previous cited ILCs types where these effects are negligible.[8-13]

Another extremely interesting, yet unexplored, class of ILCs is that in which the ionic functionality is integrated into the anisotropic core.[8-13,20-22] This arrangement may give raise to functional materials with unconventional properties, such as in the case of extended π-conjugated cores, where the coupling of the electronic semiconducting properties of the core with the ionic conductivity typical of ILCs, leads to π-conjugated ionic liquid crystals (π-ILCs) with bulk electrochromic and electrofluorescent properties.[23-25] For this class of ILCs, either columnar or smectic phases[20-21] have recently been reported but, to the best of our knowledge, only one example of π-ILCs forming nematic columnar (Nc) phase is known.[14] Nematic discotic (N_D) and

nematic columnar mesophases are characterized by typical arrangements shown in Chart 1. In N_D the long axes of the flat molecules forming the discoid are oriented parallel to a general plane (long-range orientational order), but having orientational and translational degrees of freedom along their short axes (absence of positional order). The Nc phase is instead formed by columns oriented along a preferred direction (long-range orientational order) and among which a short range positional order is established. These arrangements result in more fluid mesophases than the columnar ones.[10,12] The unique advantage offered by π-ILCs lies on their ability to self-assemble into ordered structures that may result in the enhancement of specific functionalities, for exploitation in diverse technological fields such as electrochemical (batteries, ion transistors, light-emitting electrochemical cells, etc.) and optoelectronic devices (organic photovoltaics, polarized fluorescence, electrofluorescence, light-emitting electrochemical cells), where the control of film orientation and morphology is highly desirable.[26-28] For all practical applications, therefore, it is worth to design π-ILCs exhibiting nematic phases, in order to have more affordable ways to uniform the director alignment.[29]

Chart 1. Possible nematic arrangements of disc-like mesogens.

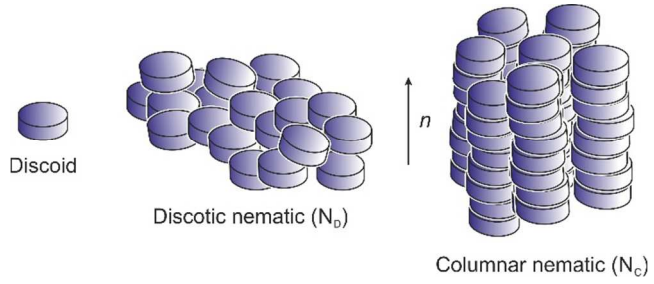

Here we study the mesomorphic properties of thienoviologen salts 4,4'-(2,2'-bithiophene-5,5'-diyl)bis(1-alkylpyridinium) as a function of the counterion type and the length of the

promesogenic alkyl chains (Scheme 1). Notably, a rich mesomorphism is afforded by a systematic change of the counterion type, leading to a wide range of new mesophases, including the nematic columnar (N_C) and discotic (N_D) ones, never observed in the homologous series of bistriflimide and iodide thienoviologen salts.[20-21] Moreover, we analyze the effect of the mesophase on the bulk fluorescence properties of these liquid crystalline materials and show, for the first time, the bulk fluorescence of a nematic phase of ionic liquid crystals.

EXPERIMENTAL SECTION

Synthetic procedures and products characterization. 4,4'-(2,2'-bithiophene-5,5'-diyl)bis(1-alkylpyridinium) iodide were prepared as previously reported.[20] The other 4-4'-(2,2'-bithiophene-5,5'-diyl)bis(1-alkylpyridinium) salts were prepared as reported in the Scheme 1 and as described in detail in Supporting Information. All other materials were commercially available and used without further purification. The compounds were characterized by ^{1}H and ^{13}C NMR spectroscopy, ESI mass spectrometry, and elemental analysis.

^{1}H NMR spectra were recorded at 25 °C in MeOH-d4 or DMSO-d6 on a Avance 300 Bruker NMR spectrometer at 300 MHz or on a Avance 500 Bruker NMR spectrometer at 500 MHz with Me_4Si as internal standard. ^{19}F NMR spectra were recorded at 25°C in DMSO-d6 on an Avance 500 Bruker NMR spectrometer at 471 MHz with CF_2Br_2 as internal standard. Chemical shifts (δ) and coupling constants (J) are given in ppm and in Hz, respectively. IR spectra were taken with a Shimadzu IR Affinity -1S spectrometer. Microanalyses were carried out with a Thermo-Fischer Elemental Analyzer Flash 2000. Mass spectra were obtained using a Thermo-Fisher LTQ XL mass spectrometer equipped with a turbo ion spray ionization source in the positive mode (ion

spray voltage 4000 V; curtain gas 35 psi; temperature 25°C; ion source gas 15 psi; declustering and focusing potentials 50 and 400 V, respectively).

Polarizing optical microscopy (POM), differential scanning calorimetry (DSC), thermogravimetric analysis (TGA) and X-Ray powder diffraction (XRD). Mesomorphism was studied by POM, DSC and XRD. Mesophases were identified by observation of sample microscopic textures using a Leitz Laborlux 12 POL polarising optical microscope in conjunction with a Linkam LTS350 heating stage. DSC thermograms were recorded with a DSC apparatus Mettler DSC-822, operating in a flowing N_2 atmosphere 10°C min^{-1} scanning rate. DSC data were treated, if it was necessary, by a deconvolution algorithm to produce separated Gauss shape curves related to the different thermic events using the software of the DSC apparatus.

TGA measurements were performed using an analytical thermobalance PerkinElmer TGA 4000, operating at heating rate of 10°C/min in air atmosphere.

X-ray powder diffraction data were collected with an automatic Philips diffractometer equipped with a variable temperature camera Anton Paar TTK450 equipped with a Standard sample holder for measurements in reflection geometry (depth 500 μm), using Ni-filtered Cu Kα radiation (λ=1.5418Å), at a continuous scanning rate of 0.1°(Δ2θ)/14.3s(Δt) with 2θ the diffraction angle. The samples were heated and cooled stepwise at a rate of 10°C min^{-1} to the appropriate temperature, and diffraction data were recorded immediately after reaching the selected temperature. The diffraction profiles have been indexed manually and refined using the program LCDiXRay for columnar liquid crystals.[30]

Photophysical properties. Steady-state photophysical investigation was performed with a HORIBA Jobin-Yvon Fluorolog-3 FL3-211 spectrometer equipped with a 450-W xenon arc lamp, double-grating excitation and single-grating emission monochromators (2.1 nm mm^{-1} dispersion; 1,200 grooves mm^{-1}) and a Hamamatsu R928 photomultiplier tube. Measurements in solution were performed at room temperature using spectrofluorimetric grade solvents.

Measurements in the bulk phase were performed on thin films obtained by filling glass sandwich cells with the material in the isotropic liquid state by capillary action. The liquid crystalline cell, was then placed into the fluorimeter sample holder on a customized temperature-controlled hotstage (CaLCTec s.r.l., Rende, Italy), with a temperature uncertainty of ±1°C. Measurements were performed in a front face geometry.

Emission and excitation spectra were corrected for source intensity (lamp and grating) and emissions spectral response (detector and grating) by standard correction curves. Time-resolved measurements were performed using the time-correlated single photon counting option on the Fluorolog 3. Details on instrumentation and method can be found elsewhere.[16,18]

The emission quantum yields of the samples were obtained by means of a Labsphere optical Spectralon integrating sphere. Sphere dimensions, sphere accessories, measurement methods and emission quantum yield determination are described elsewhere.[23,25] Absorption spectra were recorded with a Perkin Elmer Lambda 900 spectrophotometer.

RESULT AND DISCUSSION

Molecular design and synthesis. We initially investigated the effect of different counterions of the thienoviologen dication 4'-(2,2'-bithiophene-5,5'-diyl)bis(1-alkylpyridinium)$^{2+}$ bearing a C10 carbon alkyl chain, and we synthesized the thienoviologen triflate **10V(OTf)**, tosylate

10V(OTs), hexafluorophosphate **10V(PF_6)** and tetraphenylborate **10V(BPh_4)**. New thienoviologens were prepared via the quaternization reaction of 5,5-bis(4-pyridyl)-2,2'-bithiophene with appropriate iodoalkane followed by the counterion exchange (Scheme 1 and Supporting Information).

By a preliminary analysis under POM, we noticed that the compound **10V(PF_6)** did not show any type of mesophase. Probably the hexafluorophosphate anion provides too strong interactions with the cation, leading to compounds with a stable crystalline phase. On the other hand, tetraphenylborate anion is too large and may destabilize the formation of a stable dimeric structure that, as we will see forward, is the fundamental self-assembling unit of these compounds. Interestingly, however, the triflate **10V(OTf)** and tosylate **10V(OTs)** showed a liquid crystalline behavior which began at about 150°C and was maintained up to the clearing temperature of about 190°C for triflate and 280°C for tosylate (Table S1). The wide range of mesophases observed with these compounds, prompted us to study also the effect of the *N*-alkyl chains length, on the mesomorphism. To this aim, we synthesized the nonyl and undecyl thienoviologen triflate derivatives **9V(OTf)**, **11V(OTf)** and the nonyl and undecyl thienoviologen tosylate derivatives **9V(OTs)**, **11V(OTs)**.

Scheme 1. Synthesis of thienoviologen salts 4,4'-(2,2'-bithiophene-5,5'-diyl)bis(1-alkylpyridinium).

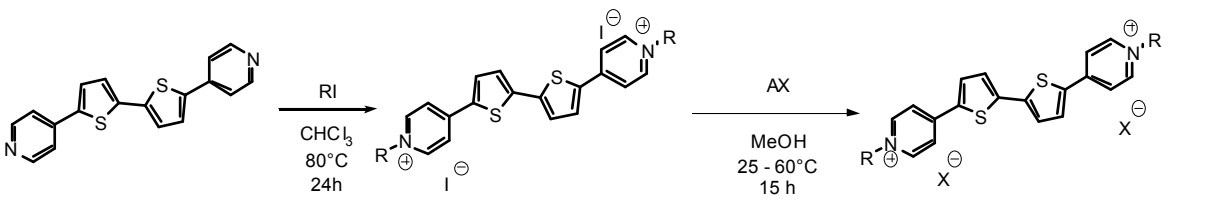

9V(I): R = $(CH_2)_8CH_3$ (64%)
10V(I): R = $(CH_2)_9CH_3$ (49%)
11V(I): R = $(CH_2)_{10}CH_3$ (47%)

9V(OTf): R = $(CH_2)_8CH_3$ X = OTf (73%)
10V(OTf): R = $(CH_2)_9CH_3$ X = OTf (78%)
11V(OTf): R = $(CH_2)_{10}CH_3$ X = OTf (82%)
9V(OTs): R = $(CH_2)_8CH_3$ X = OTs (79%)
10V(OTs): R = $(CH_2)_9CH_3$ X = OTs (72%)
11V(OTs): R = $(CH_2)_{10}CH_3$ X = OTs (84%)
10V(PF_6): R = $(CH_2)_{10}CH_3$ X = PF_6 (56%)
10V(BPh_4): R = $(CH_2)_{10}CH_3$ X = BPh_4 (92%)

AX = LiOTf, AgOTs, KPF_6, $NaBPh_4$

DSC and POM analyses. All samples were analyzed in the "as prepared" state recording the first heating and cooling DSC cyclic scans and successive thermal cycles. The samples show in the first heating scan a broad endothermic peak at temperatures lower than 100°C followed by multiple peaks at higher temperatures due to the complex polymorphic behavior and formation of mesophases typical of these systems[16,21] (curves a-c of Figure 1 A,B). The low temperature endothermic peak of as prepared samples (curves a-c of Figure 1 A,B) is absent during the second heating scan (curves a'-c' of Figure 1 A-B), indicating the presence of highly defective and imperfect crystals or solid mesophases that do not crystallize by cooling form the isotropic melt.

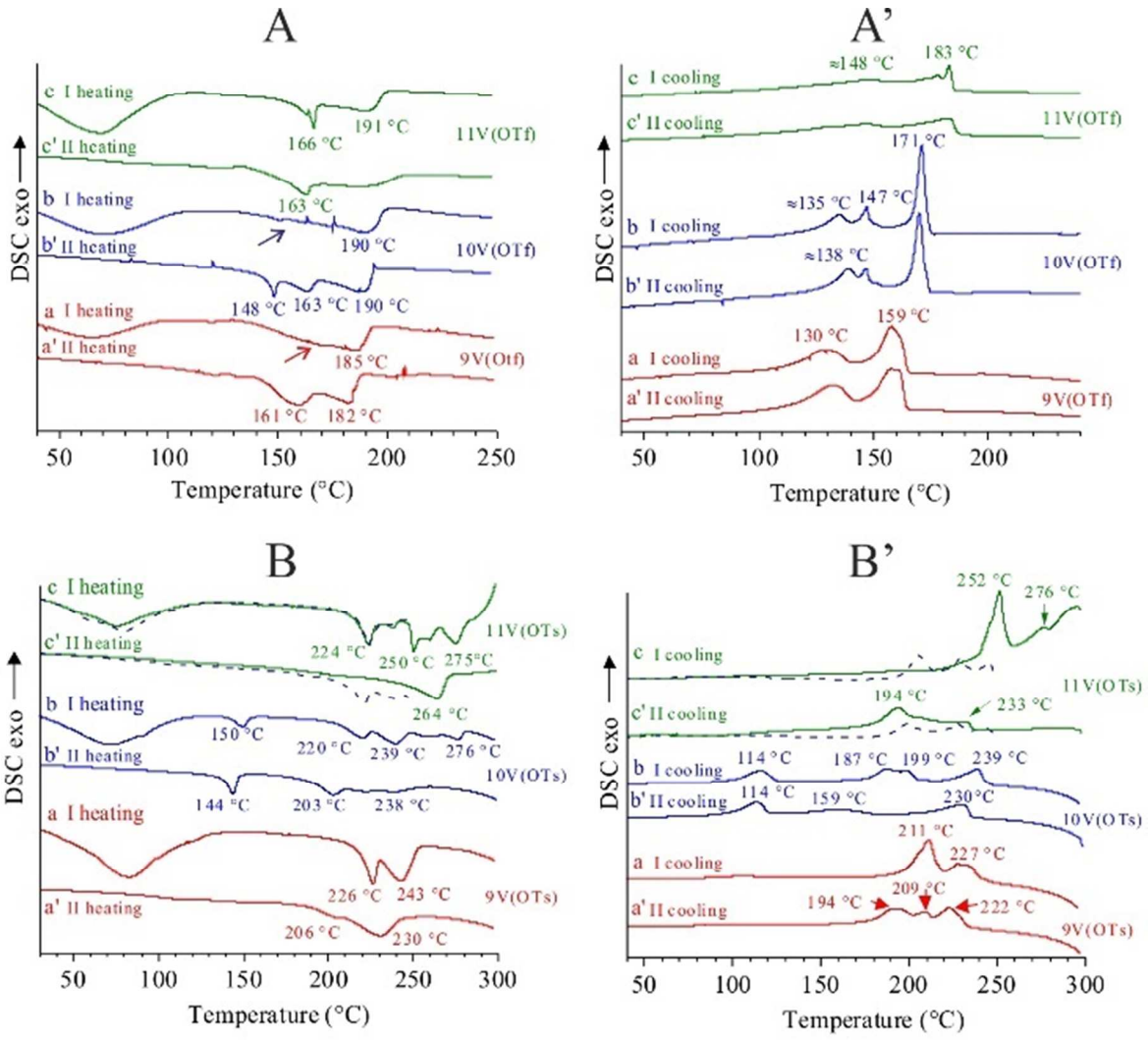

Figure 1. DSC thermograms of thienoviologen triflates (A, A') and tosylates (B, B') characterized by alkyl chains bonded to pyridyl groups of n = 9, 10 and 11 carbon atoms recorded during consecutive scanning cycles of heating (A, B) and cooling (A', B') at 10°C/min. In B and B' dotted lines indicate thermograms of the sample **11V(OTs)**, heated up to the maximum temperature of 250°C instead of 300°C. Arrows in A indicate shoulders in the long tail region of the principal peak.

The endothermic transformations occurring during the first heating scan at temperatures higher than 100°C are due to formation of mesophases before isotropization. They are also broad and produce multiple peaks or a single peak with a shoulder in the long tail region extending in the

low temperature range. The presence of multiple peaks in the high temperature range characterizes also the behavior of the samples in the second heating scan (curves a'-c' of Figure 1 A-B) and the first and second cooling steps (Figure 1 A'-B'), attributed to the formation of mesophases. As already observed in the case of bistriflimide salts of our thienoviologen dications,[13,16,20,21] we observe a general tendency of the clearing point to shift toward higher temperatures with increasing the length of *n*-alkyl moieties due to the increase of the anisotropy (Table S1 and DSC analysis in the Supporting Information). The thermal behavior of thienoviologen triflates and tosylates shows however several differences, due to the different kind of supramolecular interactions established between the dications and the bulky counterions. First, the relevant phase transitions in tosylates series occur in a temperature range higher than in the series of triflate salts. For instance the isotropization temperature of triflate salts are lower than 200°C, whereas those of the tosylates are higher than 230°C (Table S1). This shift is due to the better interactions, probably involving the aromatic rings, that the tosylate anions are able to establish with the mesogenic dications.

A second difference consists in the fact that the first and consecutive DSC thermal cycles are nearly identical in the case of triflates, indicating a reversible thermotropic behavior (Figure 1A-A'), while remarkable differences are observed in the case of tosylates (Figure 1B-B'). In fact, in the case of thienoviologen tosylates, the high temperature behavior of the samples in the second heating scan (curves a'-c' of Figure 1 B) is different from that occurring in the first heating scan (curves a-c of Figure 1 B) with a tendency of the peaks either to disappear or to shift toward lower temperatures. These differences are confirmed also in the cooling behavior (Figure 1B') and indicates that some transformations are irreversible. These irreversible processes are induced by effect of the high-temperatures reached in the first heating scans (curves a-c of Figure 1B). In

fact, heating scans performed without reaching isotropization (dashed curves c,c' of Figure 1 B,B') produce reversible phase behavior (see DSC, Supporting Information). As indicated by thermogravimetric measurements (Figure S1) and further confirmed by FTIR analysis (Figure S13-S15, vide infra), all samples show high thermal stability, with negligible weight loss and degradation, up to ≈300 °C. Therefore, the disappearance of some mesophases in the cooling scans may not be attributed to thermal degradation but is essentially the result of the high rigidity of the mesogenic cores which have low mobility and, as a consequence, difficult self-assembling ability in the molten state.

The rich thermotropic behavior of thienoviologen triflate and tosylate salts has been investigated by POM. The thin film layers of the thienoviologen triflates, formed by drop casting, show very small birefringent crystals of polygonal shape in a disordered mosaic texture at room temperature. During the first heating scan, a change in birefringence is observed at 150°C, 180°C and 190°C respectively for **9V(OTf)**, **10V(OTf)** and **11V(OTf**), in good agreement with the first endothermic peaks found in DSC (Figure 1Aa-c). This change is associated to a softening of the crystalline state which undergoes no significant alteration up to the last endothermic DSC peak corresponding to the clearing points, respectively observed at 198°C, 205°C and 216°C (Figure 1Aa-c). From the isotropic liquid (IL) state, in a reverse manner, close to the first DSC exothermic peaks (Figure 1A'a-c), a mosaic texture characterized by star-shaped domains on a pseudoisotropic background, appears at 165°C in the case of **9V(OTf)** (Figure 2a), while typical mosaic textures appear for **10V(OTf)** and **11V(OTf)** respectively at 182°C and 194°C (Figure 2c). Upon further cooling of **9V(OTf)**, **10V(OTf)** and **11V(OTf),** respectively at 130°C, 145°C and 165°C, close to the second exothermic DSC peaks (Figure 1A'a-c), the isotropic regions are progressively filled by a focal-conic texture in the first two cases (Figure 2b) or form a uniform

monolayer of mosaic texture in the latter case. No further change is observed until room temperature in the case of **9V(OTf)**, in agreement with the absence of peaks in the thermograms (Figure 1A'a), while the appearance of striations in the mosaic texture of **10V(OTf)** and a change in birefringence in the case of **11V(OTf)** occur respectively at 153° (135 °C ?????) C and 136°C. These transformations occur close to the last DSC peaks (Figure 1A'b-c) indicating sample crystallization.

9V(OTf) and **10V(OTf)** exhibit the same thermotropical behavior in all the successive thermal cycles (Figure 1Aa-b and 1A'a-b). In contrast, compound **11V(OTf)** shows a double mesomorphism on the second cooling scan from the IL state (Figure 1A'c'), with the initial formation of both mosaic texture and bâtonnetes at 206°C (Figure 2d). On further cooling across the first DSC exothermic peak (Figure 1A'c'), they slowly coalesce into an optical texture showing both fan-shaped and mosaic domains (Figure S2) which undergo a change in birefringence with the appearance of striations, indicating crystallization at 145°C.

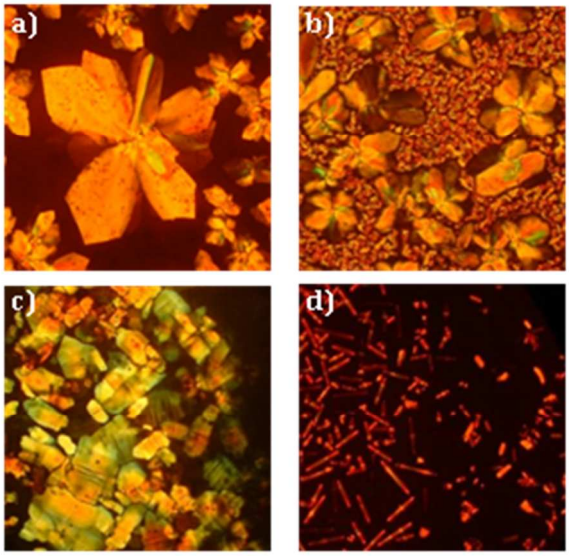

Figure 2. Optical textures acquired on cooling from the IL state for **9V(OTf)** at 165°C (a) and at 130°C (b); and for **11V(OTf)** at 194°C in the I cooling scan (c) and at 206°C in the II cooling scan (d).

The observation under POM of the thienoviologen tosylates is most challenging due to the high temperatures reached to bring the samples to isotropization (above 270°C, Table S1) for the formation of uniform thin films of the materials. Moreover, prolonged exposure of **10V(OTs)** and **11V(OTs)** at these temperatures causes the deposition of a yellow-fluorescent layer on the glass observation window of the Linkam. Since the weight loss up to 300°C is minimal (Figure S1B), this could indicate a partial sublimation of the sample, although small degradation by effect of the prolonged permanence time at 300°C may not be excluded. The thienoviologen tosylates show birefringent crystals at room temperature which undergo no transformations up to the temperature corresponding to the first sharp DSC endothermic peaks of **9V(OTs)**, **10V(OTs)** and **11V(OTs**), at 226°C, 150°C and 224°C, respectively (Figure 1Ba-c), when a change of birefringence due to a softening of the crystalline state occurs for all the compounds. Upon further heating, relevant transformations take place: at 245°C in the case of **9V(OTs)**, in correspondence of the second DSC endothermic peak (Figure 1Ba), a focal-conic texture mixed with bâtonnetes; at 250°C in the case of **10V(OTs)**, after the third DSC endothermic peak (Figure 1Bb), a focal-conic texture (Figure S4a); and at 273°C in the case of **11V(OTs)**, just after the second DSC endothermic peak (Figure 1Bc), a typical mosaic texture (Figure 3a). **9V(OTs)**, **10V(OTs)** and **11V(OTs)** undergo no further transformation up to the clearing point respectively observed at 260°C, 270°C and 285°C (Figure 1Ba-c). On cooling from the IL state, all the tosylates show the formation of bâtonnetes, respectively at 240°C, 265°C and 280°C, in agreement with the first DSC exothermic peaks (Figure 1B'a-c). At 210°C, in correspondence with the last DSC exothermic peak (Figure 1B'a), **9V(OTs)** undergoes a transition to a mosaic/marbled texture. Below this temperature, the crystalline state takes slowly the place of

the liquid crystalline state, remaining unaltered until room temperature (Figure S3). The second thermal cycle shows analogous behavior, excepted for a slight change in birefringence at 195°C, where a third exothermic peak appears (Figure 1B'a'). On further cooling below the transition observed by DSC (239°C, Figure 1B'b), compound **10V(OTs)** undergoes a transition to a fiber-like texture (Figure 3b), which transforms into a fiber-mosaic texture (reminiscent of van Gogh brushes) below 200°C (Figure S4b), according to the DSC trace showing a double transition in the range 199-187°C (Figure 1B'b). Moreover, a clear birefringence change is observed below 114°C in correspondence to the last thermal peak (Figure 1B'b), probably due to a crystallization (Figure S4c). In the second heating scan (Figure 1Bb'), this texture undergoes no change until 215°C, close to the second DSC endothermic peak (Figure 1Bb'), at which it transforms to the fiber-like texture observed in the first cooling scan, which undergoes no change until clearing at about 280°C. On cooling, neither bâtonnetes nor the fan-shaped texture occur. Instead, a new texture appears at 265°C, characterized by large domains of fibers arranged in bundles (Figure S4d), which remained almost unaltered until room temperature. In the case of compound **11V(OTs)**, a fully developed fan-shaped texture is observed at 250°C, below the highest transition reported in the thermogram of Figure 1B'c. Another significant change in the optical texture is found at 209°C, close the peak found at 205°C (Figure 1B'c, dashed curve) when a striated fan-shaped texture appears. At the same temperature, in another sample area close to that just described, a marbled texture is observed (Figure S5). This situation remains almost the same until room temperature, except that for slight birefringence changes. On heating above 255°C the sample started to melt and, before the clearing point (about 285°C), the formation of focal-conics is observed. In the second cooling, at 277°C, the formation of bâtonnetes as well as of lancets, characterizes the transition from the IL state to the high temperature liquid crystalline phase,

which leads to the formation of a mixed fan-shaped/mosaic-marbled texture (Figure 3c). Below 250°C, the marbled texture becomes predominant and, at 208°C, striations across the fans occur in the fan-shaped domains (Figure 3d), in agreement with the DSC thermogram relative to the II cooling (Figure 1B'c').

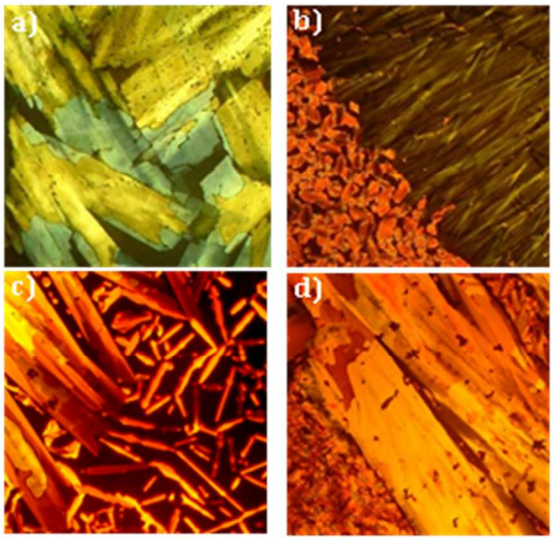

Figure 3. Optical textures observed for sample **11V(OTs)** in the I heating scan at 273°C (a) and in the II cooling scan from the IL state at 277°C (c) and (d); and for sample **10V(OTs)** at 233°C in the I cooling scan (b).

X-ray diffraction analysis. The structural transformations and the mesomorphism developing in the series of thienoviologen triflates and tosylates with temperature were investigated by X-ray diffraction analysis. We recall that the molecular units of our thienoviologens tend to form disk-like dimers (discoids) with the rigid cores having an elliptical cross section, and the alkyl chains constituting the fringes (Figure S6A),[20,21] that tend to form columnar phases (Figure S6A').[20,21] Columnar phases originate from the self-assembly of the elliptic dimers in columns packed parallel on a two-dimensional lattice, but without long-range positional correlations along the

columns.[31] As an example, the columnar rectangular arrangement of dimers according to different symmetries[32] are shown in Figure S6B-D.

Structural analysis of thienoviologen triflate salts. The X-ray powder diffraction profiles of thienoviologen triflates are shown in Figures 4, 5 and S7-S9, whereas the unit cell parameters are collected in Table S2. The indexing scheme is detailed in Table S3 of Supporting Information. In all cases, the thienoviologen triflate units form disk-like dimers (discoids, Figure S6A) organized in rectangular columnar mesophases (Col) in the pristine (as prepared) state. These solid mesophases[33] are characterized by a high degree of structural disorder. Since the structural transformations occurring in the first heating step of pristine samples up to isotropization (Figure S7-S9) are not reproduced in the successive cooling/heating steps, the details of phase changes of as prepared samples are discussed in the Supporting Information. Here we focus on the structural changes that occur in cyclic steps of cooling and heating that follow the isotropization of the pristine sample.

In the case of the sample **9V(OTf)**, the diffraction profiles recorded during the first cooling step (Figure 4A), starting from the isotropic liquid, at temperatures close to the first exothermic peak at 160°C (Figure 1A'a), present up to five order of diffraction corresponding to a smectic (lamellar) periodicity of ≈ 25 Å (SmC or SmA phase). A small reflection at $d \approx 4.4$ Å ($2\theta \approx 21°$, starred in Figure 4A), corresponding to the intra-columnar correlation spacing D of the columnar aggregates (reflection (001) of Figure S6A'), is also apparent in the diffraction profile recorded at 160 - 170°C of Figure 4A, indicating formation of small columnar stacks (Figure S6A). Correspondingly, a mosaic-like texture, characterized by star-shaped domains is observed in the POM images of Figure 2a acquired at 165°C, probably due to the high tendency of dimeric

aggregates to form columnar mesophases more easily in the thin layered films used for POM observations than in bulk.

On further cooling to 140°C, the 001 correlation peak typical of columnar stacking becomes more evident (Figure 4A). In this case, the additional presence of peaks at $d \approx 25,12,8,6$ and 5 Å ($2\theta \approx 3.5, 7, 11, 14$, and 18°), roughly corresponding to five diffraction orders for a periodicity of about 25 Å, suggests that columnar stacks are organized in a lamello-columnar phase Col_L, in agreement with the focal-conic texture observed at 130°C of Figure 2b. However, the mismatch of the spacing of these reflections from those of a perfect unidimensional (lamellar) periodic structure, and the presence of extra-reflections at $2\theta \approx 14$ and 18° (Table S3), indicates that the type of mesophase may be also considered rectangular columnar with nearly identical axes (a_r = 24.7 Å, b_r = 24.9 Å), including a high degree of disorder.

The successive cooling to temperatures lower than the crystallization temperature of 130°C leads to rectangular columnar mesophases Col_r, with Z (number of salt units/cross section) =4, (possible symmetry *p2mg*, Figure S6C and Table S3) as indicated by the diffraction profiles at 90 and 25° C of Figure 4A.

In the II heating (Figure 4B), the major change consists in the gradual intensity decrease of the reflection at $d \approx 30$ Å ($2\theta \approx 2.9°$) of the Col_r mesophase obtained in the preceding cooling step. Close to the DSC peak at ≈ 160°C (Figure 1Aa' and Table S2) only the reflection at $d \approx 24$ Å ($2\theta \approx 3.7°$) remains (Figure 4B) and the type of mesophase obtained at 170 and 185°C may be described in terms of a rectangular columnar phase (phase Col_{rd2}) with Z=4 and parameters $a_r \approx 42$ Å and $b_r \approx 31$ Å. Broad peaks of low intensity are present even at temperatures higher than the clearing (Figure 4B) as shown in the profile at 230°C. Here, the presence of broad 001 peak at $d \approx 4.5$ Å ($2\theta \approx 21°$) indicates that short columnar stacks are able to resist also above

isotropization, being characterized by some kind of order of nematic columnar type, with short-range lateral correlations as in biaxial nematic (sanidic) mesophases.[32]

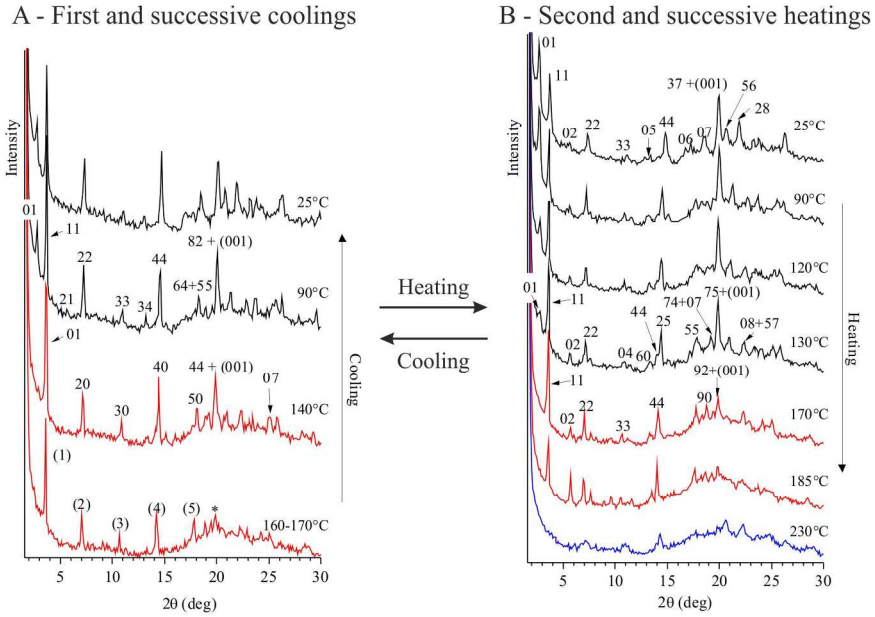

Figure 4. X-ray powder diffraction profiles of **9V(OTf)** recorded at the indicated temperatures during consecutive cooling (from isotropic state) (B) heating (C) steps after a first heating of the pristine (as prepared) sample up to isotropization (Figure S7). The *hk* Miller indices of the columnar phases are indicated (Table S3). The 001 reflection (d =4.3-4.5 Å, 2θ ≈ 20°), associated with the intra-columnar correlation distance (D) (Figure S6A), is indicated. In B, (n) indicates the n-th reflection order of a smectic mesophase.

From now on, the phase transformations occurring during consecutive cycles of cooling/heating are identical to those of Figure 4A, B. We also notice that the smectic and lamello-columnar mesophases are not obtained during heating, but form only from the IL state, during the cooling steps. We argue that once a solid mesophase with large mesomorphic domains is formed from the IL state at room temperature, it tends to keep its structure up to the clearing, probably due to

the low mobility of the bulky dications and anions. The low mobility prevents any structural rearrangement during the heating scans, so that lamellar order (smectic and lamello/columnar) are not obtained.

The mesomorphism of the samples **10V(OTf)** is illustrated in Figure S8 and described in detail in the Supporting Information. Also in this case, the thienovologen triflate units tend to form disk-like dimers (discoids, Figure S6A) organized in rectangular columnar mesophases Col_r (Figure S6). However, at variance with the sample **9V(OTf)**, the mesomorphism of the salt **10V(OTf)** consists in the absence of smectic and lamello-columnar mesophases, and in a major tendency to form rectangular mesophases, both on cooling and heating steps (see Supporting Information).

Finally, in the case of the sample **11V(OTf),** ordered columnar mesophases made of large coherent domains are obtained after the first heating step of the pristine sample up to isotropization (Figure S9) both during the first cooling (diffraction profiles at 100 and 170°C of Figure 5A) and successive heating (diffraction profiles at 175°C of Figure 5B, see Table S3). However, as shown in Figure 5C, the mesophase that develops upon cooling the isotropic liquid in the second cooling step is not columnar. For instance, the profile recorded at 170°C of Figure 5C shows only diffraction peaks at $2\theta > 5$ and a sharp reflection at $d \approx 4.4$ Å ($2\theta \approx 20°$), whereas at low angles only diffuse scattering around $2\theta \approx 3\text{-}4°$, corresponding to a correlation distance of ≈ 24 Å, is present. This corresponds to a nematic columnar mesophase N_c (Chart 1) and, as indicated by the diffuse scattering in the low 2θ region (Figure 5C), it includes some kind of lateral order of the elliptic discoids (as in biaxial nematic mesophases),[32] and some kind of smectic-like arrangement in the short range forming cybotactic regions. Therefore, in agreement with POM observations (Figure 3c,d), the sample **11V(OTf)** shows a different kind of

mesomorphism between the first and successive cooling scans from the IL state (Figure S9), with the formation of a rectangular columnar mesophase Col_r characterized by a mosaic textures (curve at 170°C of Figure 5A and Figure 3c) in the first cooling scan, and a nematic columnar N_c mesophase (curve at 170°C of Figure 5C), visualized in the presence of bâtonnetes (Figure 3d), in the second cooling scan. Upon further decrease of the temperature to 100 and 25°C, the nematic columnar phase N_c transforms into a lamello-columnar Col_L mesophase with only short range order in the lateral packing of the columnar stacks in agreement with the fan-shaped texture of Figure S2 observed at 160°C on the II cooling scan. The $N_c \rightarrow Col_L$ is reversible, and in the successive heating step, the phase changes of Figure 5C occurs in reverse order.

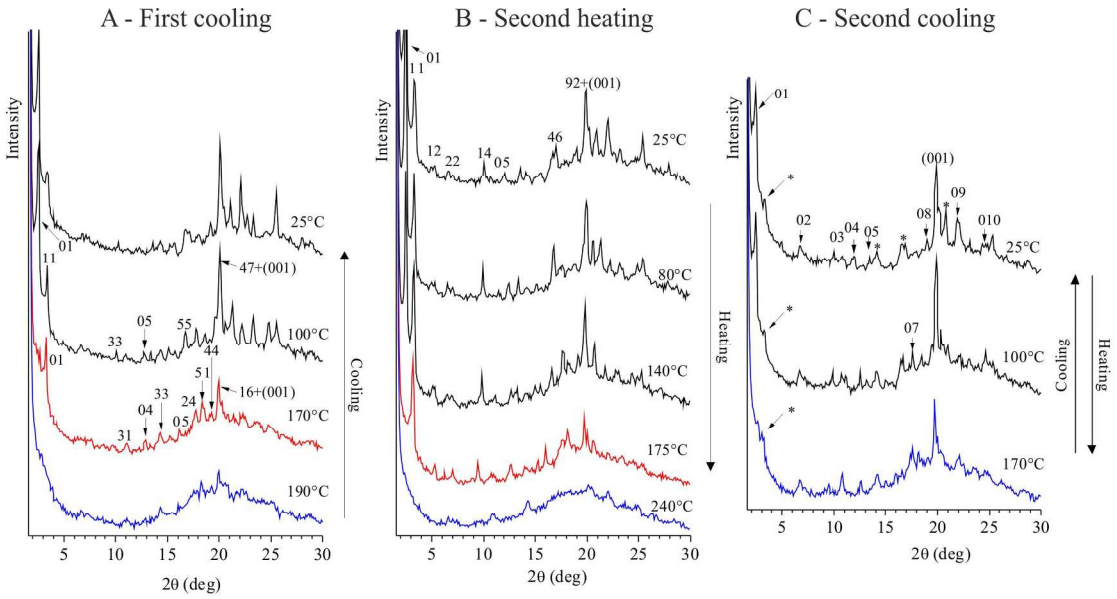

Figure 5. X-ray powder diffraction profiles of **11V(OTf)** recorded at the indicated temperatures during a first cooling step from isotropic state (A), and a second heating (B) and successive cooling /heating (C) steps. The *hk* Miller indices of the columnar phases that develop during thermal treatment are indicated (Table S3). The 001 reflection at d = 4.3-4.5 Å (2θ ≈ 20°) associated with the intracolumnar correlation distance (D) (Figure S6A') is also indicated. In B,

the peaks in the low 2θ range are out of the scale to evidence the diffraction peaks at 2θ > 5°. In C diffuse scattering around 2θ ≈3-4 is indicated with an asterisk.

Based on TGA measurements (Figure S1A), the different behavior of this sample in the first and second cooling steps is not due to sample degradation, because at the maximum temperature achieved in the melt (240°C), the weight loss is minimal. Indeed, the reproducibility of the mesomorphism in the thermal cycles starting from the second cooling on (Figure 5C), together with the fact that no significant change in the FT-IR spectrum was detected after several thermal cycles (Figure S13), indicates that our systems are intrinsically disordered and the type of mesophase achieved is highly dependent on the previous thermal history, the cooling/heating rate, the residence time of the sample in the IL state and so on.

Structural analysis of thienoviologen tosylate salts. The mesomorphism of thienoviologen tosylate salts is illustrated in Figures 6, 7,and S10-S12; the indexing of diffraction peaks is reported in Table S3, whereas the unit cell parameters are reported in Table S4. In analogy with triflates the mesomorphism of tosylate salts in the pristine samples (first heating scans, Figures S10, S11A, S12) is different from that which develops in the successive heating/cooling cycles starting from the cooling step of the isotropic liquid.

The X-ray diffraction profile of the sample **9V(OTs)** collected at 230°C, upon cooling the isotropic liquid from 300°C (Figure 6A), that is at a temperature close to highest temperature exothermic peak detected at ≈ 227°C in the corresponding DSC thermogram (Figure 1B'a), shows up to seven diffraction orders of the reflection at d ≈ 26 Å (2θ ≈ 3.5°), typical of a lamellar structure, several reflections of weak intensity, indicating lateral order, and the (001) reflection at d ≈ 4.4 Å (2θ ≈ 20°), corresponding to the average periodicity of the columnar

stacks. This indicates that the mesophase developing at 230°C may be either considered as a lamello-columnar mesophase Col_L of periodicity 26 Å with some kind of lateral order, or a disordered columnar mesophase Col_r of *p2mm* symmetry with $Z = 2$, and $a_r \approx 24$ Å and $b_r \approx 26$ Å.

On further cooling to temperatures lower than the exothermic peak at ≈ 210°C (DSC curve, Figure 1B'a), to 200 up to 25°C, diffraction profiles similar to that at 230°C are obtained, but for the presence of two diffraction peaks instead than one, at d ≈26 and 32 Å (2θ ≈ 4 and 3°, respectively) corresponding to 01 and 11 reflections (Figure 6A). Therefore the solid mesophases formed at these temperatures (Figure 6A) are rectangular columnar mesophases Col_r of *p2mg* symmetry, Z=4 and unit cell parameters a_r ≈36-39 Å and b_r ≈31-33 Å (Table S4). The similar diffraction profiles of Figure 6A are in agreement with POM observations of the compound **9V(OTs)** showing a characteristic broken fan-shaped texture immediately below the IL state which remains almost unaltered on cooling to room temperature (Figure S3).

In the successive heating scan (Figure 6A), the Col_r mesophase keeps almost unaltered up to ≈230°C (DSC curve, Figure 1Ba'), in agreement with the absence of any relevant endothermic peak during the second heating scan in this temperature range. Finally, the diffraction profile recorded at 290°C (Figure 6A) reveals residual order due to a smectic mesophase with periodicity of ≈ 26 Å, similar to that obtained in the first heating scan (Supporting Information). The diffraction data obtained during the second cooling cycle (not reported) are identical to those obtained during the first cooling, indicating that after the first heating scan of the pristine sample, the transitions are reversible.

The mesomorphism of the sample **10V(OTs)** is shown in Figure S11 and discussed in detail in the Supporting Information. This sample features the organization of the discoids in rectangular

columnar mesophases Col_r at room temperature, which remain stable in the first heating scan up to 250°C, and the irreversible re-arrangement of the columnar stacks in nematic mesophases once the sample is slowly heated to high temperatures (300°) and then cooled to room temperature. The high thermal stability of the Col_r mesophases up to high temperatures is in agreement with the focal-conic texture observed at 250°C in the POM image of Figure S4a during the first heating scan of the pristine sample, whereas the irreversible re-arrangement into nematic mesophases is in agreement with the bâtonnetes, and the fiber-like textures observed under POM (Figure 4b, S4b and S4d) during the cooling scan from the IL state.

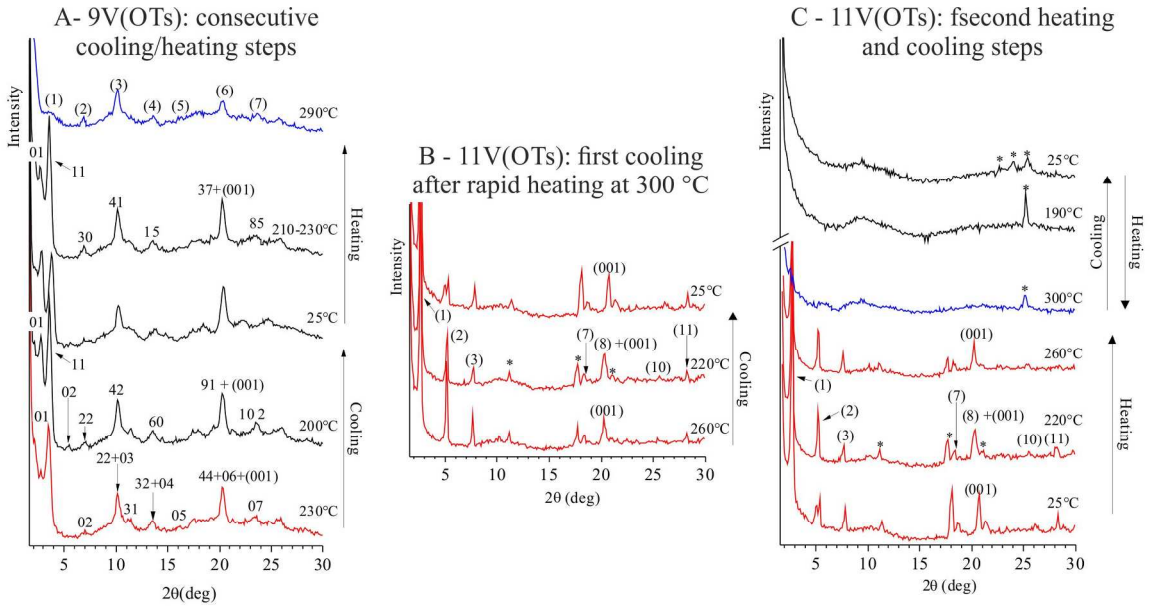

Figure 6. X-ray powder diffraction profiles of **9V(OTs)** (A) and **11V(OTs)** (B,C) samples recorded at the indicated temperatures during consecutive cooling and heating steps, following the first heating of the pristine samples (Figure S10, S12). The *hk* Miller indices of the columnar mesophases are indicated (Table S3). The 001 reflection at d =4.3-4.5 Å (2θ ≈ 20°) corresponding to the intra-columnar correlation distance (D) (Figure S6A) is also indicated. Symbols (n) indicate the n-th reflection orders of a smectic mesophase. Data in B,C are recorded

on a sample subjected to a first rapid heating up at 300°C, to prevent irreversible structural rearrangements. In B the peak at 2θ ≈ 2.4 ° is off the y-scale to evidence the weak diffraction peaks at 2θ>5°.

Finally, the mesomorphim of the sample **11V(OTs)** is shown in Figure 6B,C. This sample develops rectangular columnar mesophases Col_r only in the first heating from pristine state that, at 260°C, transform into lamello-columnar mesophases Col_L (see Supporting Information, Figure S12). Also in this case, the prolonged heat treatment from 25 to 300°C of the as prepared sample induces irreversible structural changes (Figure S12 and Supporting Information). Therefore, the transformations occurring upon cooling (Figure 6B) and the successive heating/cooling cycles (Figure 6C) have been followed also using an independent sample that has been previously rapidly heated up to 300°C and then analyzed. The mesophases of this second sample from 260 to 25°C upon cooling (Figure 6B) and in reverse order in successive heating (Figure 6C), are similar to that of Figure S12 recorded at 260°C during the first heating step of the pristine sample. In fact, all of them correspond to mesophases that are variants of a same lamello-columnar mesomorphic modification Col_L with periodicity of about 36 Å, a degree of lateral order that reversibly increases (decreases) with decreasing (increasing) the temperature, and well-formed columnar stacks of periodicity equal to 4.3-4.4 Å (Figure 6B). The formation of lamello-columnar mesphases Col_L corresponds to the different variants of fan-shaped or marbled textures observed in the POM images (Figure S5) during the first heating scan.

The diffraction profiles recorded in the successive cooling step from 300 to 25°C in Figure 6C, show two broad halos centered at 2θ ≈ 10 and 20°C along with a single broad reflection at d ≈ 3.54 Å, (2θ ≈ 25°) at high temperatures (300 and 190°C) and a triplet of broad peaks at d ≈ 3.52,

3.7 and 3.9 Å (2θ range 23-26°) at 25°C. These reflections are due to formation at high temperatures of a discotic or columnar nematic mesophase, N_D or N_C (Chart 1), in agreement with the bâtonnetes and/or lancets textures observed in the POM images of Figure 3b,c. Therefore, in the X-ray diffraction experiments, the step-by-step heating process leads to the formation of nematic mesophases at high temperatures, that are unable to evolve toward more ordered mesophases during the cooling step. As a consequence, the cooling to room temperature leads to formation of a solid mesophase with some kind of frozen-in nematic order and the initial lamello-columnar mesophases Col_L are not recovered (Figure 6C).

The diffraction data collected in the second cooling step (Figure 6C) are identical to those collected in the successive heating step in reverse order, indicating that, once the sample has experienced irreversible structural rearrangements in the slow heating process up to 300°C, all transitions in consecutive cycles of heating/cooling become reversible. Therefore, the lamello-columnar mesophases are not recovered upon cooling, but only highly disordered solid mesophases with nematic like ordered are obtained (Chart 1), characterized by aggregates experiencing strong interactions.

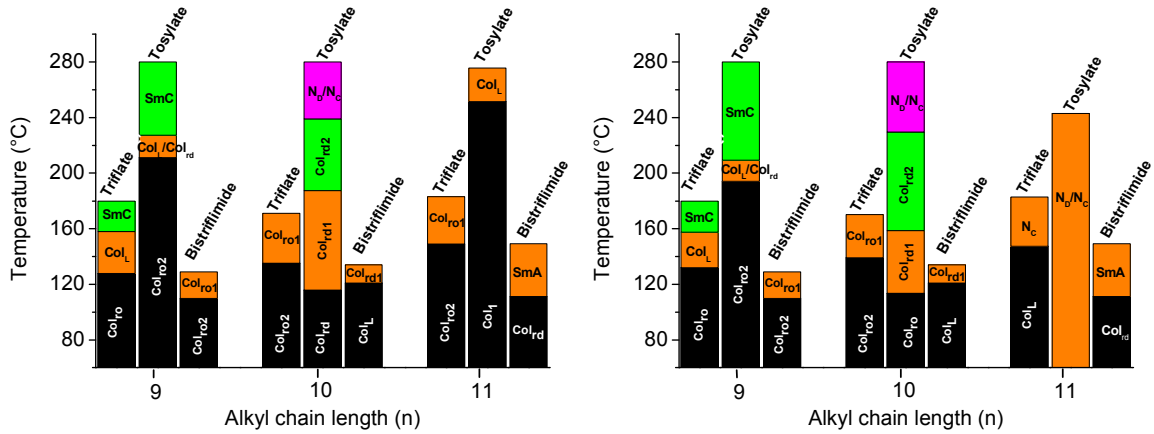

Figure 7. Dependence of the mesomorphic properties of thienoviologens on the anion type and on the length of the alkyl chain on the first (left) and second (right) cooling cycle respectively.

The complex and rich mesomorphism of thienoviologens is summarized in Figure 7, where the behavior of the thienoviologens bistriflimide previously investigated[20] has been included in order to stress the strong dependence of the mesophase on both the nature of the anion and the length of the alkyl chain.

Moreover, Table 1 reports the phase behavior and structural information observed during the second cooling scan. As already pointed out, a reversible phase behavior occurs just after the second heating scan and therefore, the information provided in Table 1 reflect the thermotropic behavior of the thienoviologens during the successive thermal cycles.

Table 1. Transition temperature, transition enthalpy values (in brackets)[a] and structure (in parenthesis) for thienoviologen triflate salts and thienoviologen tosylate salts during the second cooling scan

Compounds	Phase (symmetry) –Transition temperature (°C) [Enthalpy] (J/g) → Phase
9V(OTf)	IL — ≈180-170 [n.d.][b] →SmC — 157.5 [13.3] → Col_L — 131.9 [15.3] → K(Col_{ro}/p2mg)
10V(OTf)	IL — 170.1 [13.1] → Col_{ro1} (p2mg) — 147.0,139.1 (double peak) [12.9] → K(Col_{ro2}/p2mg)
11V(OTf)	IL — 182.9 [9.3] → N_C — 147.5 [8.0] → K(Col_L)
9V(OTs)	SmC — 222.1, 209.4 [15.9] → Col_L / Col_{rd} (p2mm) — 194.1 [13.0] → K(Col_{ro2}/p2mg))

10V(OTs)[c]	N_D/N_C (quenched)— 229.7 [8.1] → Col_{rd2} (p2mg)— 158.7 [3.8] → Col_{rd1} (p2mg) — 113.5 [5.8] → K(Col_{ro}/p2mg)
11V(OTs)	IL — 233.0 [5.9] → N_D/N_C 194.3 [15.2] → K(N_D/N_C) (quenched)

[a]Determined by DSC analysis at a scan rate of 10°C min^{-1} in the 2th cooling scan; abbreviations: K = Solid mesophase; Col_{ro} and Col_{rd} = ordered and disordered columnar rectangular phases, respectively; Col_L = Lamello-columnar phase; SmA and SmC = smectic A and smectic C phase, respectively; N_D, N_C = Discotic nematic and columnar nematic phases, respectively; IL = isotropic liquid state. The type of phases was deduced from X-ray diffraction analysis. [b]Transformation is not detectable in the DSC thermogram, n.d. = not determined. [c]These transitions occur only preventing high-temperature induced irreversible processes at 300°C. By a step-by-step slow heating process the nematic-like order of the melt at 300°C is frozen in the solid state.

Photophysical properties. All the thienoviologen compounds were characterized in diluted *N*-methyl-2-pyrrolidinone (NMP) solution as a function of the concentration. In dilute solution (10^{-6} mol L^{-1}), the absorption spectra in the UV-Vis range are fully superimposable, showing a unique band at 433 nm originated by the π-π* transition typical of charged thienoviologen species (see Figure 9 as a representative example).[21,25,33]

The emission spectra of the six compounds show a single emission band centered at 536 nm (see Figure 8 as a representative example), confirmed by the excitation spectra showing a sharp band at 433 nm, well reproduced absorption ones (see Figure S16). Due to the similarity of all the compounds in solution, differences attributable to the aliphatic chain length or the type of counterion can be excluded; this is confirmed by the emission quantum yields (Φ) and the excited state lifetimes (τ) measurements, showing Φ values ranging from 0.48 to 0.57, and decay

profiles deconvoluted by a bi-exponential function giving τ values of about 9 and 2 ns, with the last value having a weight larger than 90% (see Table S5).

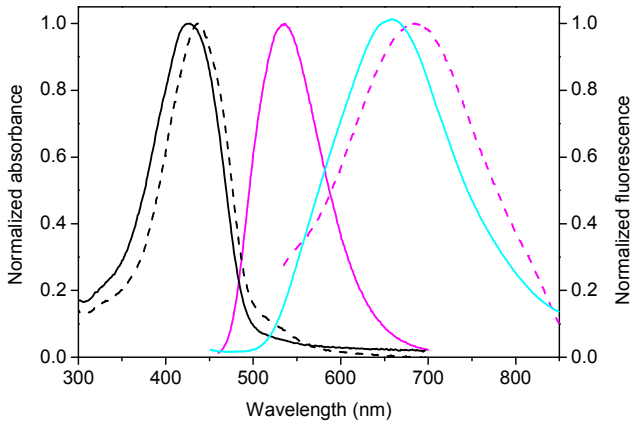

Figure 8. Absorption and emission spectra of **9V(OTf)** in dilute NMP solution (1.5×10^{-6} mol L^{-1}) (solid black and magenta lines), in concentrated solution (4.2×10^{-4} mol L^{-1}) (dotted black and magenta lines) and of **11V(OTs)** in the nematic columnar phase (cyan line).

More interesting results have been obtained when concentrated (4.2×10^{-4} mol L^{-1}) solutions were considered, as described below for the exemplary case of **9V(OTf)**. By increasing the solution concentration, a low-intense absorption band at about 520 nm is observed as a shoulder on the tail of the principal band at 433 nm (Figure 8). By exciting the high-energy band, an emission spectrum with a peak at 536 nm is observed, perfectly superimposable to that recorded from diluted solution (Figure 8). Interestingly, by exciting at 520 nm, a new emission band is observed at 680 nm extending into the near infrared region (Figure 8).

The excitation spectrum (Figure S16) confirms this behavior: if we observe the emission at 536 nm, the spectrum presents a single band at 433 nm, while, by fixing the emission monochromator at 680 nm, the band at 520 nm is still recorded together with that at 433 nm. Emission quantum

yield and lifetimes recorded at 680 nm are reported in Table 2 and are compared to those measured for the dilute solution.

As can be seen, these photophysical parameters are considerably different in the concentrated solution. In the diluted sample, a bi-exponential decay accounts for a little presence of single fluorescent species with τ = 9.6 ns, and a quenched dimeric structure with τ = 2.2 ns, contributing mainly to the green fluorescence emission band. In contrast, the red emission band occurring in the concentrated solution, is mostly determined by higher order aggregates with short lifetimes and by a little amount of dimers (τ = 3.0 ns), while the single species is absent.

Notably, these aggregates characterizes also the fluorescent properties of the thienoviologens in the bulk, as shown in Figure 8 for the nematic phase of **11V(OTs)** at room temperature. It exhibits a rather wide fluorescent emission band centered at 640 nm to which the shorter decay times mainly contribute (Table 2). Further studies, addressed to the full characterization of the fluorescence of these thienoviologens in the bulk LC state, are in progress.

Table 2. Photophysical properties of NMP solutions of 11V(OTs) as representative thienoviologen

Parameter	Solution		Fluorescent unit
	Diluted (λ_{em} = 536 nm)	Concentrated (λ_{em} = 680 nm)	
Φ/%	[a]57.64	[c]0.92	
τ/ns (A/%)	[b]2.2 (94.0)	[d]0.4 (17.0), [d]1.3 (77.0)	Aggregates
		[d]3.0 (6.0)	Dimeric structures
	[b]9.60 (6.0)		Single species

[a]λ_{ex} = 433 nm; [b]λ_{ex} = 379 nm; [c]λ_{ex} = 520 nm; [d]λ_{ex} = 620 nm.

CONCLUSIONS

Here we have shown that a variety of mesophases can be afforded in π-ILCs by tuning the intermolecular interactions responsible for self-assembling. This can be achieved simply by

changing the counterion type and/or the length of the promesogenic chains attached to the rigid core. By this strategy, we afforded nematic columnar and discotic phases, seldom observed in ionic liquid crystals, which exhibit also important fluorescent properties.

ASSOCIATED CONTENT

Supporting Information. Experimental details about the synthetic procedures, additional data on polarized optical microscopy, XRD structural analysis and photophysical properties (PDF), this material is available free of charge via the Internet at http://pubs.acs.org.

AUTHOR INFORMATION

Corresponding Author

*lucia.veltri@unical.it, *amerigo.beneduci@unical.it

Author Contributions

All authors have given approval to the final version of the manuscript.

ACKNOWLEDGMENTS

The authors thank the University of Calabria. The postdoctoral fellowship of S.C. and V.M. was co-funded by the European Commission, the European Social Fund and by the Regione Calabria in the framework of ARUE project. The authors are the unique responsible of this work and both the European Commission and the Regione Calabria refuse any responsibility on the use of the information reported here.The authors wish to thank Dr. Rocco Di Girolamo for his support in XRD data analysis and for useful discussion.

REFERENCES

(1) Cano-Sarabia, M.; Angelova, A.; Ventosa, N.; Lesieur, S. *J. Colloid Interface Sci.*, **2010**, *350*, 10-15.

(2) Angelova, A.; Reiche, J.; Ionov, R.; Janietz, D.; Brehmer, L. *Thin Solid Films*, **1994**, *242*, 289-294.

(3) Ionov, R.; Angelova, A. *Phys. Rev. E*, **1995**, *52*, R21-R24.

(4) Ionov, R.; Angelova, A. *J. Phys. Chem.*, **1995**, *99*, 17593-17605.

(5) Ionov, R.; Angelova, A. *J. Phys. Chem.*, **1995**, *99*, 17606-17614.

(6) Angelova, A.; Ionov, R. *Langmuir*, **1996**, *12*, 5643-5653.

(7) Lin, X.; Grinstaff, M.W. *Isr. J. Chem*., **2013**, *53*, 498.

(8) Binnemans, K. *Chem. Rev*., **2005**, *105*, 4148.

(9) Stappert, K.; Lipinski, G.; Kopiec, G.; Spielberg, E. T.; and Mudring, A.-V. *Cryst. Growth Des.*, **2015**, 15, 5388.

(10) Axenov, K. V.; Laschat S. *Materials,* **2011**, *4,* 206.

(11) Chen, S.; Eichhorn, S.H. *Isr. J. Chem*., **2012**, *52*, 830.

(12) Wöhrle, T.; Wurzbach, I.; Kirres, J.; Kostidou A.; Kapernaum, N.; Litterscheidt, J.; Haenle, J. C.; Staffeld, P.; Baro, A.; Giesselmann, F.; Laschat, S. *Chem. Rev*., **2016**, 116, 1139.

(13) Kouwer, H. J.; Swager, T. M. *J. Am. Chem. Soc*., **2007**, *129*, 14042-14052.

(14) Artzner,F.; Veber, M.; Clerc, M.; Levelut, A. M. *Liq. Cryst.,* **1997**, 23, 27.

(15) Yelamaggad, C. V.; Mathews, M.; Hiremath, U. S.; Shankar Rao, D. S.; Prasad, S.K. *Chem. Commun*., **2005**, 1552.

(16) Goossens, K.; Nockemann, P.; Drisen, K.; Goderis, B.; Gorller-Walrand, C.; Van Hecke, K.; Van Meervelt, L.; Pouzet, E.; Binnemans, K.; Cardinaels, T. *Chem. Mater*., **2008**, *20*, 157.

(17) Li, W.; Zhang, J.; Li, B.; Zhang, M.; Wu, L. *Chem. Commun*., **2009**, 5269.

(18) Li, X.; Lan, X.; Ma, S.; Bai, L.; Meng F.; Tian, M. *Liq. Cryst.*, **2014**, *41,* 1843.

(19) Ahn, S.; Yamakawa, S.; Akagi, K. J. *Mater. Chem. C*, **2015**, *3*, 3960.

(20) Beneduci, A.; Cospito, S.; Crispini, A.; Gabriele, B.; Nicoletta, F. P.; Veltri, L.; Chidichimo, G. *J. Mater. Chem. C*, **2013**, *1*, 2233.

(21) Cospito, S.; Beneduci, A.; Veltri, L.; Salamonczyk, M.; Chidichimo, G. *Phys. Chem. Chem. Phys*., **2015**, *17*, 17670.

(22) Pană, A.; Ilişa, M.; Staicu, T.; Pasuk, I.; Cîrcu, V.; *Liq. Cryst.*, **2015**, DOI: 10.1080/02678292.2015.1116630.

(23) Beneduci, A.; Cospito, S.; La Deda, M.; Veltri, L.; Chidichimo, G. *Nat. Commun*., **2014**, *5*, 3105.

(24) Beneduci, A.; Cospito, S.; Imbardelli, D.; De Simone B. C.; Chidichimo, G.; *Mol. Cryst. Liq. Cryst*., **2015**, 610, 108.

(25) Beneduci, A.; Cospito, S.; La Deda, M.; Chidichimo, G. *Adv. Funct. Mater.,* **2015**, *25,* 1240.

(26) O'Neill, M.; Kelly, S. M. *Adv. Mater*.,**2011**, *23,* 566.

(27) Funahashi M. *J. Mater. Chem. C*, **2014**, *2*, 7451.

(28) Wang, Y.; Shi, J.; Chen, J.; Zhu, W.; Baranoff, E.; *J. Mater. Chem. C*, **2015**, *3*, 7993.

(29) Bisoyi, H. K.; Kumar, S.; *Chem. Soc. Rev*., **2010**, *39*, 264.

(30) Godbert, N.; Crispini, A.; Ghedini, M.; Carini, M.; Chiaravalloti, F.; Ferrise, A. *J. Appl. Cryst.* **2014**, 47, 668-679.

(31) Compendium of Polymer Terminology and Nomenclature. IUPAC Recommendations 2008. RSC Publishing: Cambridge, 2009. ISBN: 978-0-85404-491-7. Chap. 6.

(32) International Tables for Crystallography, vol. A T. Hahn Ed. Springer; Dordrecht, 2002. ISBN-10: 0792365909. Part 6, p. 91.

(33) Alberto, M. E.; De Simone, B. C.; Cospito, S.; Imbardelli, D.; Veltri, L.; Chidichimo, G.; Russo, N. *Chem. Phys. Lett*., **2012**, *552*, 141-145.

For Table of Contents Use Only

Mesophase Tuning in Discotic-Dimers π-Conjugated Ionic Liquid Crystals through Supramolecular Interactions and the Thermal History

Lucia Veltri, Vito Maltese, Finizia Auriemma, Chiara Santillo, Sante Cospito, Massimo La Deda, Giuseppe Chidichimo, Bartolo Gabriele, Claudio De Rosa, and Amerigo Beneduci

Table of Contents Graphic

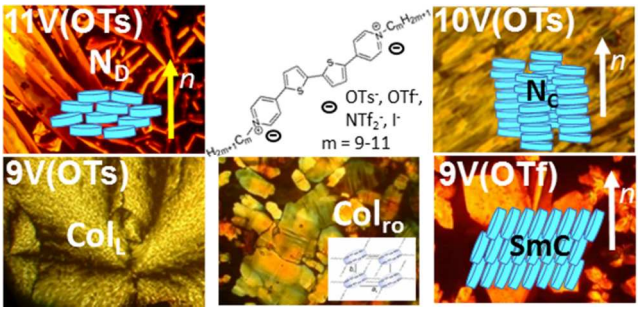

Synopsis

Mesophase tuning can be afforded in thienoviologens π-conjugated ionic liquid crystals, by tuning the intermolecular interactions responsible for self-assembling, i.e., by changing the counterion type and/or the length of the promesogenic chains attached to the rigid aromatic core

of the cation. Thienoviologens show indeed smectic, columnar as well as nematic columnar and discotic phases.